Turbulence and transport in mirror geometries in the Large Plasma Device

Phil Travis[1, a)] and Troy Carter[1]
University of California, Los Angeles Department of Physics and Astronomy

(Dated: 22 March 2024)

TODO: Finish Mirror machines are rising again as a potential class of fusion reactors, but cross-field transport and turbulence in mirrors remains relatively understudied compared to toroidal devices. Turbulence and transport in edge-like conditions in mirror configurations were studied utilizing the flexible magnetic geometry of the Large Plasma Device (LAPD). Multiple mirror ratios from $M = 1$ to $M = 2.68$ and three lengths from $L = 3.51$m to $L = 10.86$m were studied. Emphasis is placed on the impact of mirror ratio M on fluctuating quantities.

Using Langmuir and bdot probes, data were collected on fluctuating quantities in radial lines, enabling profile measurements and spectra of density, temperature, floating and plasma potentials, and magnetic fluctuations. $E \times B$-driven particle flux was calculated from these quantities. Two probe correlation techniques were used to infer wavenumbers and 2d structure.

Cross-field particle flux and density fluctuation power decreased with increased mirror ratio. Core density and temperatures remain similar with mirror ratio, but radial line-integrated density increases. No evidence of mirror driven instabilities — interchange, velocity space, or otherwise — were observed.

The physical expansion of the plasma by using a higher field in the source region may partially have caused the reduction in density fluctuation power through the increased gradient scale length. Despite the introduction of magnetic curvature, many possible stabilization methods of interchange were present.

The cold edge of a fusion reactor may not make an appreciable contribution to cross-field particle transport.

I. INTRODUCTION

With the advent of highly-funded commercial ventures and high-field high-temperature superconducting magnets, mirror machines are once again rising in prominence as a candidate for commercial fusion reactors[1,2]. Historically, mirror research has prioritized the main issues with mirror confinement: stabilizing the interchange instability, stabilizing velocity-space (loss-cone-driven) instabilities, and minimizing axial electron heat losses. Nevertheless cross-field transport remains an important topic in magnetic-confinement fusion reactor development, both in linear and toroidal geometries. Insight into edge-relevant turbulence performed in a basic plasma science device may be useful for a mirror-based reactor. Although not at fusion-relevant core temperatures or densities, the Large Plasma Device (LAPD) operates at conditions similar to the edge of fusion devices and can provide insight into the physical processes in that region.

Non-classical cross-field particle transport is often caused by low-frequency, large-amplitude fluctuations. These fluctuations are the result of various instabilities, such as the "universal" drift instability, caused by a density gradient, becoming unstable at finite resistivity. Drift wave turbulence and the effect on transport has been extensively studied in the past[3,4]. In the presence of sufficiently high rotation or sheared flow, rotational interchange and the Kelvin-Helmholtz instabilities also contribute or couple to these fluctuations.

Various gradient-, rotation-, and shear-driven instabilities (and suppression of such) have been studied previously in the LAPD experimentally[5–7] and in simulations[8]. The LAPD has a sufficiently high spontaneous rotation rate that rotation-driven instabilities may be excited without artificial drive. Simulations have suggested that a rapidly growing nonlinear instability may dominate over all other linear instabilities.

Imposing a magnetic mirror configuration introduces magnetic curvature, which may drive the flute-like interchange instability caused by a parallel pressure gradient and curvature vector. This interchange mode could couple to finite $k_{\|}$ drift waves. The coupling of drift waves to curvature-induced interchange modes has been studied in toroidal devices such as TORPEX[9,10], where curvature was seen as the driving component for the unstable drift-interchange modes. Drift-like fluctuations have also been observed in the GAMMA-10 mirror[11,12]. Flute-like modes and drift waves have been studied in other linear devices, such as Mirabelle[13], where the appearance of flute-like modes or drift waves were controlled by varying the field and limiter diameter.

Biasing or modifying the electrical connection of the plasma with the end wall has proven to be a important actuator in many mirror machines such as TMX-U[14], GAMMA-10[11], and GDT[15–17], and will be utilized on WHAM[1]. Active biasing was not attempted in this study, but the intrinsic rotation and strong electrical connection to the source region may provide a useful analog.

The LAPD exhibits a high degree of turbulence so it is difficult to identify the dispersion relation of the modes that are present. Nevertheless, the LAPD has good coverage of perpendicular spectra using correlation-plane techniques, and some measure of parallel spectra using the correlation between two axially-separated probes. A space-time spectral characterization of the many instabilities present in this low beta, moderate aspect ratio, gas-dynamic trap regime is attempted.

This paper is organized as follows: Sec. II discusses the configuration of the LAPD and diagnostics the diagnostics used; Sec. III covers the changes seen when imposing a magnetic mirror configuration on profiles, particle flux, core

[a)]Electronic mail: phil@physics.ucla.edu

and gradient region fluctuations, turbulence, and confinement; Sec. IV explores the changes in 2d (x-y plane) structure; Sec. V discusses these results in context with previous work; Sec. VI concludes the study with comments on further research needed.

TODO: Page 16-ish in Liewer 1985 describes a $\tilde{n}/n \sim \rho_s/L_n$ relationship (which is what we see in the LAPD at the edge? Check this

TODO: omega/k phase velocity for the 3kHz mode is on the order of ExB rotation velocity? – note that in the paper somewhere

II. DEVICE CONFIGURATION

A. The Large Plasma Device (LAPD)

The Large Plasma Device (LAPD) is a 20 meter long, 1 meter diameter basic plasma device at UCLA[18]. The LAPD has a variable magnetic field, from 250G to 1.6 kG and can be varied axially. Probes inserted into the plasma can collect high-resolution, temporal information on density, temperature, potential, and magnetic field fluctuations. TODO: Include simple cartoon illustrating the coordinate system used. In this study, the plasma was formed using an emissive, 60 cm diameter barium-oxide (BaO) cathode and a 72 cm diameter, 50% transparent molybdenum anode that accelerate electrons across a configurable $40-70$V potential; voltages of 60 and 63V were used in this study. The source has since been upgraded to a lanthanum hexaboride (LaB6) cathode[19] that enables access to higher-density, higher-temperature regimes.

The flexible magnetic geometry of the LAPD was used to construct a variety of magnetic mirror configurations. The discharge current, fill pressure, and other machine parameters were held constant. The typical plasma parameters observed in this study can be seen in table II.

Data in several mirror ratios and lengths were collected (see table I) but emphasis is placed on the short cell because it was able to access the highest mirror ratio possible ($M = 2.68$) with a ≈ 500 Gauss midplane field and had probes outside of the mirror cell. A overview of the axial magnetic field for the the short mirror configurations and probe locations can be seen in fig. 1. Periodic mirror configurations were also explored but are not examined in this study.

TODO: Shrink magnetic field plot vertically, add LAPD coordinate system + cathode/anode + ifo

Mirror length	Mirror ratios (M)			
Flat	1			
3.51 m (short)	1.47	1.90	2.30	2.68
7.03 m (medium)	1.49	1.98	2.46	
10.86 m (long)	1.47	1.97	2.44	

TABLE I. Magnetic mirror lengths and ratios. The lengths are measured where the curvature changes sign and the ratio is the maximum divided by the minimum. Approximately 3.5m must be added to the length if the good-curvature region is included. In the case of small asymmetries, the field strengths were averaged before calculation.

Cathode radius (M=1)	x_c	30		cm
Machine radius	R	50		cm
Plasma length	L	~ 17		m
Primary species		He-4 1+		
Electron-helium mass ratio		1.37×10^{-4}		
Neutral pressure		$6-20\times10^{-5}$		Torr
Quantity		Core	$x = x_{\mathrm{PF}}$	Unit
Density	n_e	1.25×10^{12}	0.6×10^{12}	cm^{-3}
Ion temperature	T_i	~ 1	—	eV
Electron temperature	T_e	4	5	eV
Beta (total)	β	9×10^{-4}	6×10^{-4}	
Midplane magnetic field	B_{mid}	500	—	G
Plasma freq	Ω_{pe}	10	7.1	GHz
Ion cyclotron freq	Ω_{ci}	200	—	kHz
Electron cyclotron freq	Ω_{ce}	1.4	—	GHz
Debye length	λ_D	0.013	0.021	mm
Electron skin depth	λ_e	30	43	mm
Ion gyroradius	λ_{ci}	5.8	—	mm
Electron gyroradius	λ_{ce}	0.13	0.15	mm
Ion thermal velocity	$\bar{v}_i$	6.94	—	km/s
Electron thermal velocity	$\bar{v}_e$	1190	1330	km/s
Sound speed	c_s	13.0	13.9	km/s
Alfvén speed	v_a	$446-1140$	-1620	km/s
Ion sound radius	ρ_s	65	69	mm
Ion-ion collision freq	ν_{ii}	730	380	kHz
Electron-ion collision freq	ν_{ei}	6.77	2.59	MHz
Electron collision freq	ν_{ee}	9.57	3.66	MHz
Ion mean free path	$\lambda_{i,\mathrm{mfp}}$	26	50	mm
Electron mean free path	$\lambda_{e,\mathrm{mfp}}$	175	512	mm
Spitzer resitivity	η	192	146	$\mu\Omega\,\mathrm{m}$

TABLE II. LAPD machine information and plasma parameters in the core and peak-fluctuation region ($x = x_{\mathrm{PF}}$) at the midplane in this study. Dashed quantities are assumed to be identical to core quantities.

B. Diagnostics

All diagnostics were recorded with a effective sampling rate of 6.25 MHz (16-sample time average at 100 MSPS) and a spatial resolution of 0.5 cm. When necessary, averaging over time is done in the approximate steady-state period of the plasma discharge (4.8 to 11.2 ms from the 1 kA trigger signal). Unless otherwise noted, all data presented will be from probes inside the mirror region ($z \approx 7$m).

The data presented were collected in two phases. The first phase ("datarun"), `DR1`, collected Langmuir probe (I_{sat} and Vf) and magnetic fluctuation ("bdot") traces. 50 shots were taken at each position for every configuration. The second phase, `DR2`, was conducted with a similar set of diagnostics focused on temperature measurements (swept and triple probe) and 2d x-y structure. 15 shots were taken at each position, except for Langmuir sweeps with 64. When appropriate, all data for each position were averaged over these shots.

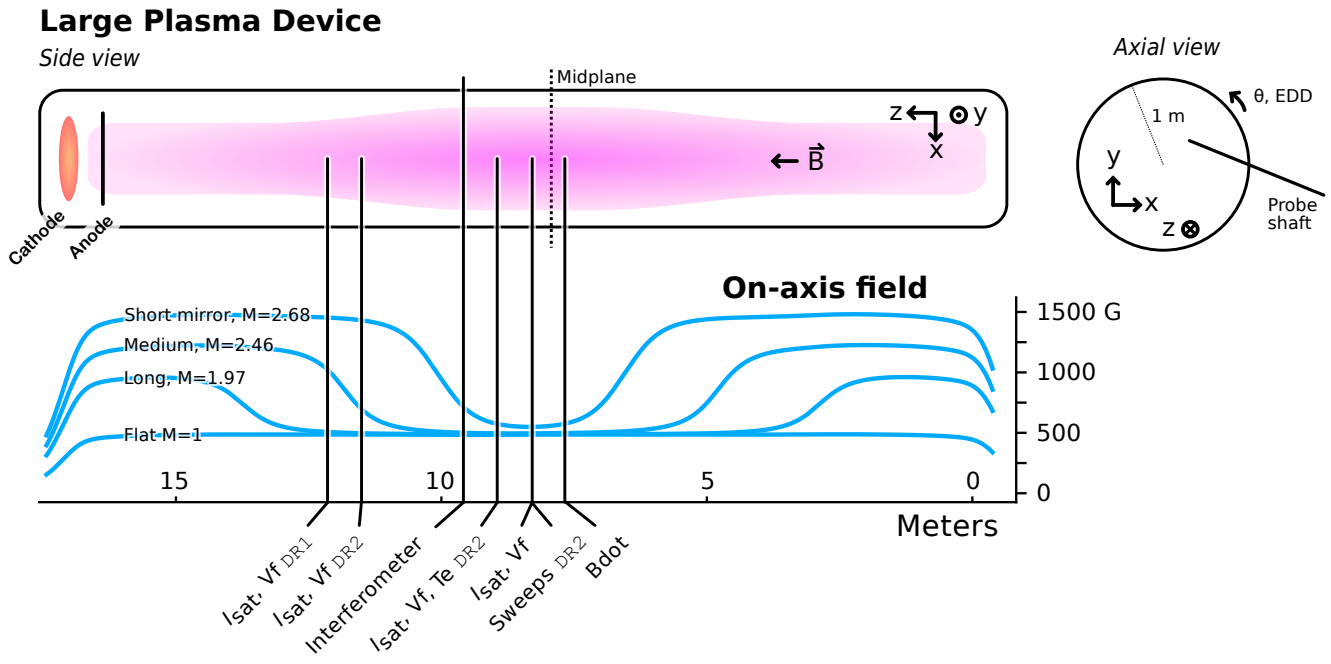

FIG. 1. Axial magnetic field profile for short mirrors, with the diagnostics used in the first datarun labeled.

III. MIRROR-INDUCED CHANGES

A. Bulk profile modification

Because the field of the plasma source is increases with M, the midplane plasma expands by a factor of $\sqrt{M}$. This expansion leads to broader plasma profiles and decreased core density but maintains similar to the magnetically-mapped cathode radius x_c as seen in fig. 2. The line-integrated density as measured by a 56 GHz heterodyne interferometer increases up to $\sim 35\%$ (fig. 3) but does not increase past a mirror ratio of 2.3. This leveling-off of density and a lack of change in plasma decay time (from the interferometer time series) suggests that this line-integrated density increase is caused largely by an increase in plasma volume, not by improved confinement TODO: sus – see comments on confinement . Discharge power increases only slightly (3%) at higher mirror ratios suggesting negligible impact on density. Langmuir sweeps and triple probe measurements of T_e (DR2) show slightly depressed core and slightly elevated edge T_e with increasing mirror ratio (fig. 4). Plasma potential decreases across the plasma (fig. 5) when the mirror ratio exceeds 1.9. This drop in plasma potential may be caused by the anode becoming grounded to the wall, which should begin at $M = 1.93$ given the 72 cm anode and 100 cm vessel diameters. This potential profile creates a sheared $E \times B$ velocity profile (fig. 5 limited to 500 m/s in the core and exceeding ~ 3 km/s at the far edge. The floating potential (Vf) profile also exhibits similar behavior but is excluded for brevity.

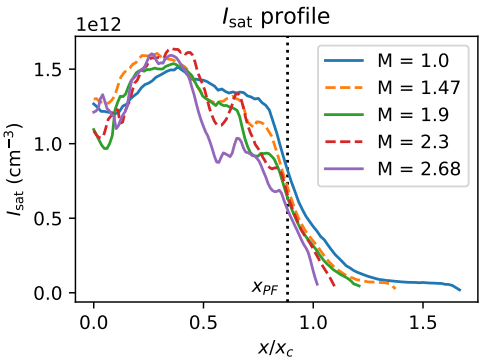

FIG. 2. I_{sat} profile (assumed $T_e = 4.5$ eV). Effective area was calibrated using a nearby interferometer.

B. Particle flux and density fluctuations

The density fluctuation power peaks at the steepest gradient region ($x_{PF} = x/x_c \sim 0.88$) as expected as seen in fig. 6. x_{PF} occurs at nearly the same magnetically-mapped coordinate for each mirror ratio. These density fluctuations are the primary driver of the cross-field particle flux. Vf fluctuations also peak at the same location, but the total power across mirror ratios are similar and, relative to density fluctuations, much lower in the core. Core density fluctuations below 2 kHz are substantial in the core at lower mirror ratios, possibly caused by hollow profiles, but are outside the scope of this study.

A spectral decomposition technique is used to calculate the

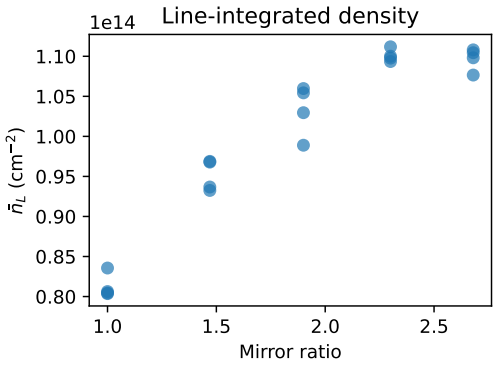

FIG. 3. Line-integrated density as measured by a 56 GHz interferometer as a function of mirror ratio, taken from four discharges for each mirror configuration. Density increases up to a mirror ratio of 2.3 where it appears to level off.

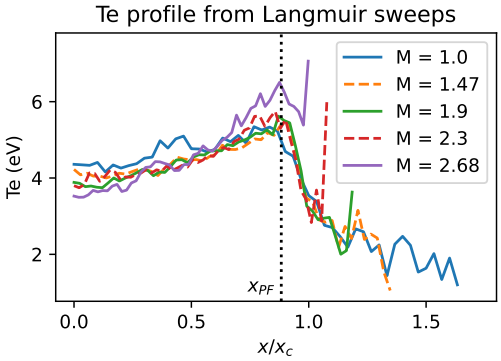

FIG. 4. T_e from Langmuir sweeps (DR2). Triple probe results are nearly identical. The increased temperatures directly at the plasma edge are likely artifacts caused by sheath expansion in lower densities.

time-averaged particle flux[20] as seen in fig. 7:

$$\Gamma = \langle \tilde{n}\tilde{v} \rangle = \frac{2}{B}\int_0^\infty k(\omega)\,\gamma_{n\phi}(\omega)\sin(\alpha_{n\phi})\sqrt{P_{nn}(\omega)\,P_{\phi\phi}(\omega)}\,d\omega \quad (1)$$

where k is the azimuthal wavenumber, γ is the coherency, α is the cross-phase, and P the power spectrum. This method is more robust than the naive time-integration of $n(t)\cdot\tilde{E}(t)$ because it accounts for the coherency of the density-potential fluctuations. This representation also enables inspection of each contributing term in the event of surprising or problematic results. A plot of the I_{sat}-Vf phase can be seen in fig. 8. The flattened particle flux in the core is likely caused by primary electrons (emitted from the cathode) destroying the spatial localization of the Vf measurement, so Vf fluctuations are no longer proportional to plasma potential fluctuations[21]. Azimuthal wave number is measured by two Vf probe tips 0.5 cm apart. This technique yields good agreement with correlation plane measurements. The $\tilde{E}\times B$ particle flux clearly decreases with mirror ratio; most of this decrease is attributed

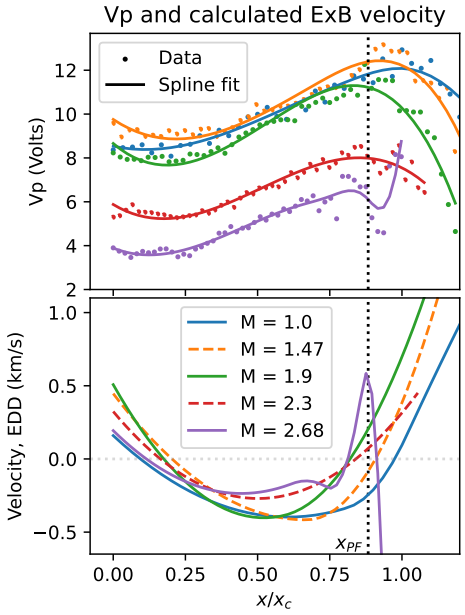

FIG. 5. Plasma potential and derived $E\times B$ velocity profiles from Langmuir sweeps. $x/x_c > 1.2$ has been excluded from the graph for greater clarity in the core and gradient region. The electric field was calculated by taking the gradient of the spline-smoothed plasma potential profile.

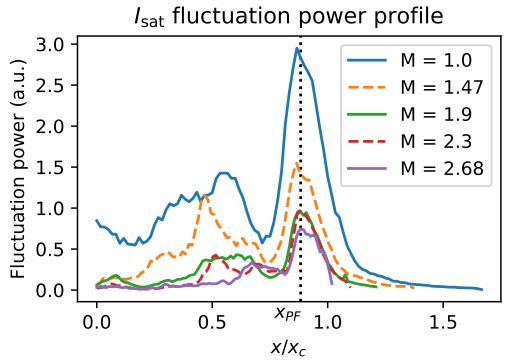

FIG. 6. I_{sat} profiles for signals 2 kHz and up. The lower frequency components associated with bulk profile evolution dominate the core region and are not the focus of this study.

to the decrease in density fluctuation power. The particle flux for each mirror ratio was normalized to the area of an equivalent solid angle in the $M = 1$ case to compensate for the increased plasma surface area at the same magnetically-mapped coordinate x/x_c. This particle flux is on the order of Bohm diffusion $D_B = \frac{1}{16}\frac{T_e}{B} \approx 6.25\text{m}^2\text{s}^{-1}$ as observed in other transport studies[22].

T_e profiles and fluctuations may affect particle fluxes but measurements of both were not taken in the same datarun. Nontheless, a quantification of the effect of T_e on particle flux is attempted. T_e fluctuations affect I_{sat}-based density measure-

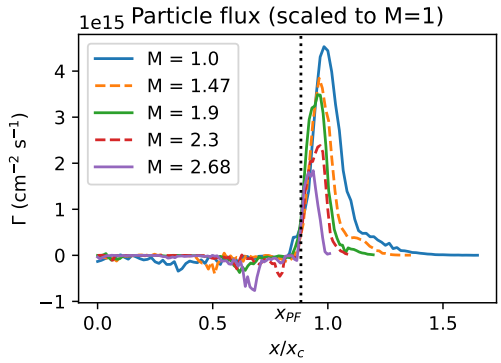

FIG. 7. Cross-field, $\tilde{E} \times B$ fluctuation-based particle flux with respect to mirror ratio. A monotonic decrease in particle flux is observed with increasing mirror ratio. Particle flux is normalized by solid angle to the $M = 1$ area to account for the geometry-induced decrease in particle flux caused by a larger-diameter plasma.

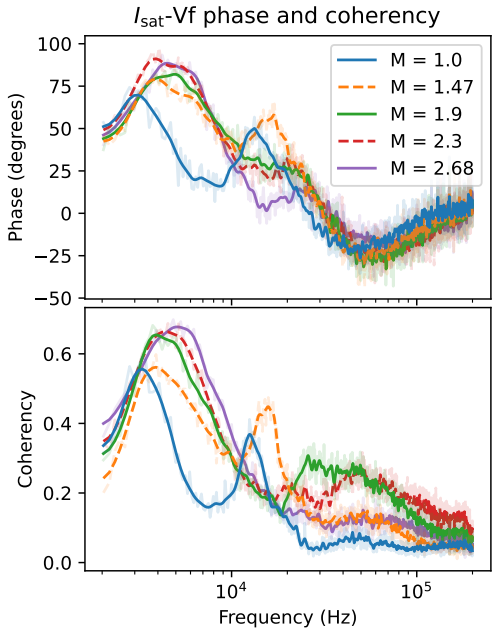

FIG. 8. Phase and coherency of I_{sat} current and Vf near x_{PF}, smoothed. Positive phase means I_{sat} leads Vf.

ments through the $T_e^{-1/2}$ term, and triple probe and Langmuir sweep T_e measurements suggest that temperature gradients have a negligible impact. A naive incorporation of temperature fluctuation data from DR2 into particle fluxes from DR1 suggest that cross-field particle flux may be underestimated by up to 50% via the I_{sat} temperature term, but the trend and relative fluxes across mirror ratios remain unchanged. Such a naive incorporation should be treated with suspicion because of the sensitive nature of the flux with respect to the gradient and the differences in profiles between DR1 and DR2. These difference in profiles made be caused by cathode condition, deposits on the anode, or a different gas mix and are difficult

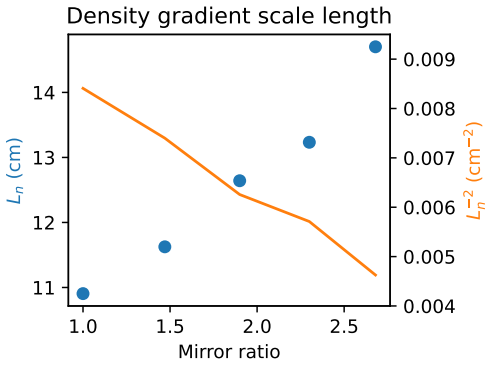

FIG. 9. Gradient scale length L_n and the associated term in the drift wave growth rate L_n^{-2}. This scale length was calculated over a 3 cm region around x_{PF} (peak fluctuation region).

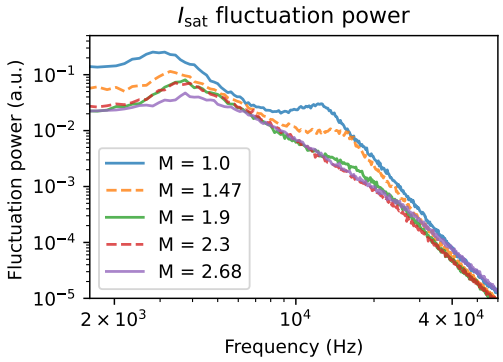

FIG. 10. I_{sat} (density) fluctuation power averaged over a 3 cm region around x_{PF}. The fluctuation power is largely featureless beyond 40 kHz aside from electronics noise.

to account for.

The reduction in particle flux (fig. 7) is roughly corresponds to the reduction in the drift wave growth rate by the term L_n^{-2} as seen in fig. 9. Thus, the reduction in particle flux can be partially explained away by the increased scale length but a causal link cannot be established without further experiments, such as creating a mirror without midplane plasma enlargement.

C. Gradient-region fluctuations

The I_{sat} fluctuation power spectra in the region of peak power $x \sim x_{\text{PF}}$, also where the density gradient is strongest, can be seen in fig. 10. Notably, the fluctuation peaks shift to higher frequencies and decrease in total fluctuation power. The shift in frequency may be the decrease in the Doppler shift caused by the spontaneous $E \times B$ plasma rotation seen in fig. 5. The phase angle of I_{sat} and Vf provides insight into the nature of the driving instability. Including a nonzero resistivity η in the drift wave leads to a small phase shift δ between

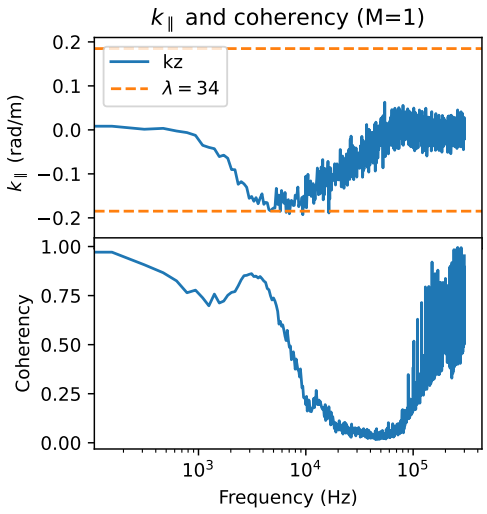

FIG. 11. $k_\parallel$ and coherency γ as a function of frequency. Only results from the $M = 1$ case are available, but it is clear that there is a long, 40m, wavelength mode identified at 3 and 12 kHz as a drift and drift-Alfvén wave, respectively.

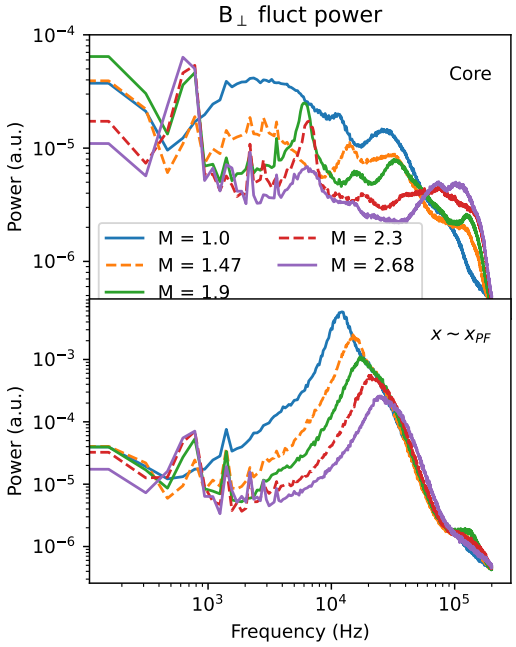

FIG. 12. $B_\perp$ fluctuation power around the peak fluctuation point ($x \sim x_{PF}$) and the core (0-15 cm). Fluctuation power decreases across the board with mirror ratio except for core frequencies close to Ω_{ci}. Peaks around $10-30$ kHz at x_{PF} are consistent with drift-Alfvén waves and the near-cyclotron frequency features in the core may be resonating Alfvén waves created by the magnetic mirror.

density and potential. phil: This bit is new: The phase shift δ between density and potential for drift waves in collisional plasmas is on the order of $\delta \approx \omega\nu_e/k_\parallel^2 v_e^{23}$. Plugging in typical values ($k_\parallel = 0.15$, $\bar{v}_e = 1200$ km/s, $\nu_e = 6$ MHz, $\omega = 3$ kHz) yields a substantial phase shift $\delta \approx 32°$, which roughly agrees with the phase shifts in fig. 8, though the implied increased phase shift at higher frequencies does not agree with measurements. As seen in fig. 8, the phase shift between I_{sat} and Vf fluctuations are large below 20 kHz, suggesting the presence of additional modes beyond or significant modification of resistive drift wave fluctuations.

TODO: Redo calculations/plot but with 34m wavelength instead of 40 The phase difference between two Vf probes, 3.83 m apart, was used to calculate the parallel wavelength $\frac{2\pi}{\lambda} = k_\parallel = \phi_{\text{Vf1, Vf2}}/\Delta z$ assuming the wavelengths are greater than 7.66 m. The two probes mapped to the same field line only in the $M = 1$ configuration, so parallel wavenumbers are available only for the flat case. A 34 m wavelength mode exists from 3 to $\sim$ 10 kHz (fig 11. Drift waves are long-wavelength modes so coherent density and potential fluctuations along the flux tube are expected. The coherency is a measure of similarity of the spectral content of two signals, in this case Vf probes 1 and 2. The coherency is defined as $\gamma = \frac{|\langle P_{1,2}\rangle|}{\langle |P_{1,1}|^2\rangle\langle |P_{2,2}|^2\rangle}$ where $P_{x,y}$ is the cross-spectrum between signals x and y and the angle brackets $\langle\rangle$ denote the mean over shots. The coherency between the two Vf probes drops off with increasing frequency, with a slight bump at around 12 kHz. There are several candidates for the driving mechanism of the 3 kHz mode, but the 12 kHz mode is most likely a drift-Alfvén wave.

The perpendicular magnetic fluctuation ($B_\perp$) component of this drift-Alfvén wave can be clearly seen in fig. 12. These $B_\perp$ fluctuations are spatially and spectrally coincident with the electrostatic fluctuations (fig. 10). phil: Feedback in this section below would be appreciated Drift-Alfvén waves have been studied in the LAPD in the past[23,24]; strong coupling is observed for $\beta_e > m_e/m_i$. The Alfvén speed $\omega/k_\parallel = v_A = B/\sqrt{4\pi nM}$ (given $\omega \ll \Omega_{ci}$) when averaged over the entire column ranges from $\sim$ 444 to $\sim$ 1348 km/s. A $k_\parallel$ corresponding to a wavelength $\lambda = 40$m TODO: redo calculation falls within the bound established by the kinetic and inertial Alfvén wave dispersion relations at the frequency peaks observed at $x \sim x_{PF}$ seen in fig. 12. The lengthening of field lines caused by curvature accounts for at most 10% of the change in frequency. The dispersion relation for oblique ($k_\perp \gg k_\parallel$) Alfvén waves when including the Hall effect in Ohm's law is[25,26]:

$$\begin{aligned} \omega &= -i\gamma_0 \pm \sqrt{\omega_0^2 - \gamma_0^2}, \text{ where} \\ \omega_0 &= k_\parallel v_A \sqrt{\frac{1+k^2\rho_s^2}{1+k_\parallel^2 v_A^2/\Omega_{ci}^2 + k^2\lambda_e^2}}, \\ \gamma_0 &= \frac{1}{2}\frac{\eta k^2}{1+k_\parallel^2 v_A^2/\Omega_{ci}^2 + k^2\lambda_e^2} \end{aligned} \tag{2}$$

where the relevant quantities are defined in table II. The inclusion of the Hall term is necessary because $k_\perp\rho_s \sim k_\perp\lambda_e \sim 1$ at the frequency ranges of interest (fig. 16). At the peak $B_\perp$ frequencies, this dispersion relation yields purely damped modes. TODO: This part needs the calculations double checked too: The increasingly damped Alfvén waves in this

region could be a contributing factor to the decreased fluctuation amplitude of the drfit-Alfvénic turbulence phil: This piece above really needs another set of eyes! I'm pretty much throwing everything at the wall and seeing what sticks.

D. Core magnetic fluctuations

TODO: Make plot showing scaling of the core, high-frequency feature with field strength and cell length. One feature of note is the increase in $B_\perp$ fluctuations (fig. 12) in the core right below the cyclotron frequency ($66 \lesssim \omega \lesssim 200$ kHz): this the only fluctuating quantity to *increase* with mirror ratio. The frequency of this feature scales inversely with mirror length TODO: reference plot here . This feature is speculated to be a shear-Alfvén standing wave because of these scalings with the field configuration and its absence in the flat case. These standing waves have been observed in the magnetosphere TODO: cite and in the LAPD in the source region as an Alfvén wave maser[27].

The sub-1 kHz modes in $B_\perp$ and its harmonics are nearly constant in power across the entire plasma; these features are likely perturbations from the magnet power supplies.

E. Turbulence modification

The wavenumber-power relation in fig. 13 shows decreased fluctuation power when a mirror configuration is introduced, but an increased mirror ratio had little effect. The greatest decrease in fluctuation power occurred in low and high k_y's, around 10 and 70 rad/m. The shape of the power-k_y curve does not follow an exponential distribution, and only for a small portion of the curve is it consistent with a 2d drift-wave cascade (Wakatani Hasegawa k^-3)[28]. The steep dropoff in fluctuation power with k_y suggests that higher-wavenumber fluctuations do not have a significant effect on transport. Core turbulence fluctuations appear to decrease dramatically as seen in the I_{sat} fluctuation power (fig. 10) and is supported by the I_{sat} decorrelation time increases from ~ 0.7 ms for $M = 1$ to ~ 2.5 ms for $M = 2.68$. At $x = x_{PF}$, decorrelation times for all mirror ratios remained at 0.2 ms.

F. Confinement

Troy: This is a strong claim to lead with – having not done particle balance calculations, it's hard to defend this. For example, the mirror field could lead to decreased ionization rate at the same input power, but the density doesn't increase because the confinement is actually better! . No noticeable change in confinement time is observed.

phil: Might just axe this whole section. Confinement time would be straightforward if the temperature doesn't drop so quickly. I could take a look at the probe data on very short timescales after the discharge cuts off. TODO: Look at temperature+isat decay

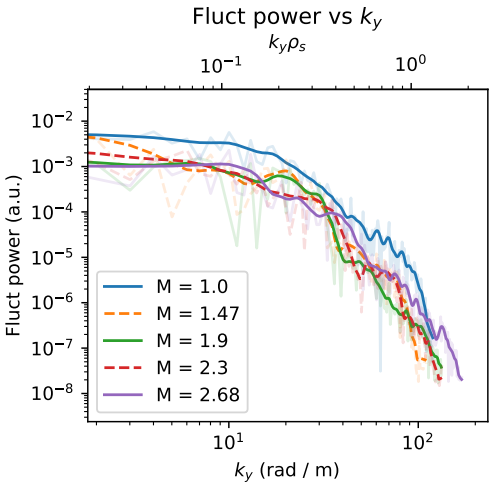

FIG. 13. Fluctuation power summed for each k_y for frequencies up to 100 kHz, smoothed. The contribution to fluctuation power is negligible past 100 kHz. The turbulent k_y spectrum is nearly identical across mirror ratios.

Interferometer time traces at $z = 9.58$m show no change in decay rate. Immediately after the discharge is terminated, the line-integrated density decays exponentially: $\exp -t/\tau$, where τ is between $14.55 - 15.42$ms and does not correlate with mirror ratio TODO: the temperature does rapidly drop so check that . phil: Axial density losses dominate over radial[7,22] .

Preliminary results with the upgraded LaB6 cathode show obvious enhanced confinement in mirror or half-mirror configurations, which may be the result of entering new regime.

IV. 2D STRUCTURE

The perpendicular magnetic field is calculated by phase-aligning each frequency at each position using a stationary reference Langmuir probe (DR2). The phase-aligned perpendicular magnetic field vectors ($\vec{B}$) and the corresponding axial current density structure (j_z) for the flat-field ($M = 1$) case can be seen in fig. 14. The current is derived from the magnetic field via $\nabla \times \vec{B} = \mu_0 j$. Two main current channels can be seen with the magnetic fields circulating around them. This structure quickly decoheres in time as expected in a turbulent plasma. At higher mirror ratios, the field magnitude and corresponding current density decrease (which was also seen in DR1: fig. 12).

Using two, axially-separated, correlated I_{sat} measurements (DR2), the azimuthal mode number m (radially integrated) was calculated. Higher-frequency and higher-m features are seen with increasing mirror ratio (fig. 15). This higher-m trend suggests that azimuthal structures do not scale with increased plasma radius but instead remain roughly the same size. The limited planar probe movement caused an increase

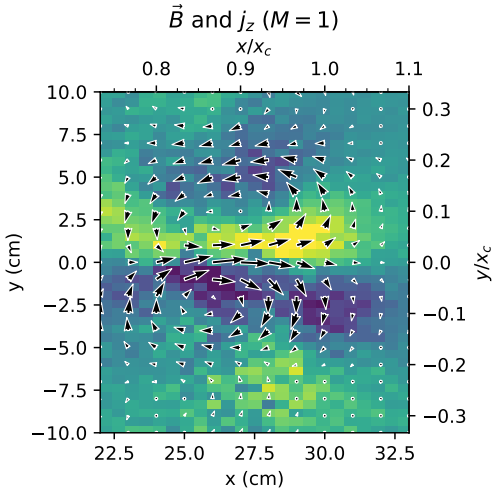

FIG. 14. Perpendicular magnetic field and the derived current density for the flat-field ($M = 1$) case using a bodt probe with an axially-separated I_{sat} reference (DR2).

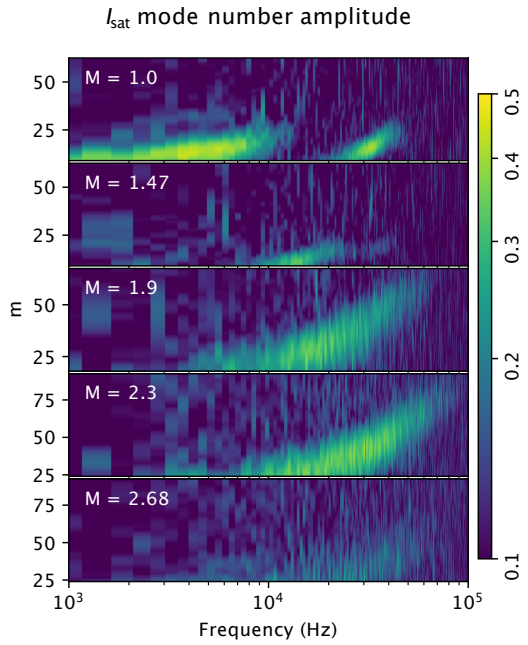

FIG. 15. Azimuthal mode number m amplitudes calculated from two axially-separated, correlated, I_{sat} probes. Increasing mirror ratio leads to increased m at higher frequencies. (DR2)

in the lower bound on m in higher mirror ratios. At mirror ratios 1.47 and higher, the lower frequency component (< 10 kHz) appears to decrease significantly in amplitude. Calculating $k_\perp$ from m evaluated at $x \sim x_c$ yields similar k_y values as the two-tip technique (16). The average k_y for a given frequency can be calculated using two Vf tips on the same probe by calculating the phase difference and dividing by the spatial separation of 5 mm: $k_y = \phi_{\mathrm{vf1,\,vf2}}/\Delta y$[29]. The maximum $|k_y|$

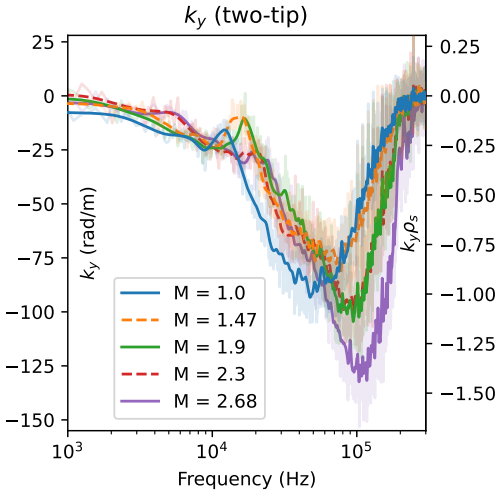

FIG. 16. k_y averaged about x_{PF} and smoothed for each mirror ratio calculated using two vertically-separated Vf tips on the same probe. Little change is seen in k_y at lower frequencies but higher frequencies tend towards larger k_y at higher mirror ratios.

measurable before aliasing is $\pi/\Delta y \approx 628$ rad/m. As seen in fig. 16, the k_y spectrum remains similar across mirror ratios, but the wavenumber extends further into higher frequencies with increasing mirror ratio.

V. DISCUSSION

A. Lack of mirror-driven instabilities

No evidence is seen for mirror-driven instabilities — curvature, loss-cone, or otherwise. Given the LAPD parameters in this study (tables I and II), the collision frequencies are sufficiently high such that the mirror is in the gas-dynamic regime: losses out of the mirror throat are governed by gas-dynamic equations rather than free streaming through the loss cone. To be in the gas-dynamic regime, the mirror length must exceed the mean free path of the ions[30]:

$$L > \lambda_{ii} \cdot \ln M / M \tag{3}$$

where L is the mirror length, λ_{ii} is the ion mean free path, and M is the mirror ratio. These collisions populate the loss cone and maintain a (cold) Maxwellian distribution, eliminating the possibility of loss-cone-, ion-driven instabilities like the AIC[31] or DCLC[32,33] instabilities that have been observed in other (historic) devices.

The back-of-the-envelope interchange growth rate is approximately[34,35]

$$\Gamma_0 = \frac{c_s}{\sqrt{L_M L_P}} \tag{4}$$

which yields $\Gamma_0 \approx 1.2$ kHz using $L_M \approx 7$m and $L_P = 17$m (c_s is used instead of $\bar{v}_i$ because $T_i \ll T_e$ and mirror length L is

split to distinguish between the contributions of the plasma length and mirror length to inertia and to curvature drive, respectively). Interchange does not appear because the aspect ratio of these mirrors is quite large, limiting the growth rate of interchange, and line-tying to the cathode further lowers the growth rate. The hot cathode used for plasma formation functions as a thermionic endplate that can supply current to short out the flute-like interchange perturbations. Line-tying has been seen in flux rope experiments on the LAPD using a hotter, denser source[36], also in other devices[37], and is why interchange was not seen in the earliest mirror machines[34]. Note that the plasma terminates on the cathode or end plates before the magnetic field flares out, so there is no contribution to stability from an expander tank as seen in other GDTs[30,35]. Given the low (~ 1 eV) ion temperatures, finite Larmor radius effects are negligible. If interchange were visible, there would be an new, obvious, low-frequency mode in I_{sat} fluctuations when the mirror curvature or plasma pressure is sufficiently increased.

Interchange could also be at least partially stabilized by the continuous production of electrons in the core that are electrostatically trapped by the ambipolar potential[38]. The intuition behind this stabilization mechanism is that new electrons are continuously created, and any change in the local potential will cause more or fewer electrons to be lost out the ends of the device along that field line, counteracting the potential change. This stabilization mechanism has been experimentally demonstrated to completely suppress interchange when the ambipolar potential $\Phi \gtrsim 6T_e$[39].

The $E \times B$ shear flow present (fig. 5) may also make a contribution to the stabilization of interchange via vortex confinement[15–17,35]. The estimated shearing rate is between 3.3 and 10 kHz, which is greater than the estimated ≈ 1.2 kHz growth rate of the interchange mode.

B. Potential instabilities driving turbulence

Rotational interchange can be significant driver of the broadband turbulence spectrum in the LAPD, particularly when a biased limiter is installed. This observation has been confirmed by both linear simulations[40] and biasing experiments[7]. This mode is flute-like (as seen in fig. 11) and is characterized by a phase between density and potential of around 45 to 90° which is consistent with the phase measurements seen in fig. 8. The rotational interchange mode could couple with the drift wave at $k_\parallel = \pi/L \sim 0.37$ rad/m ($n = 0.5$), which has been observed in the past[7] and likely present here. TODO: Make plots (or at least do the calculations) of the phi/Te and nfluct/n and compare them (Schaffner's thesis page 133; Jassby 1972, also in Brochard 2005) . Estimates of shearing rate from the $E \times B$ flow velocity profile (fig. 5) suggest that the shearing rate is sufficiently low that the Kelvin-Helmoholtz turbulence drive is not significant TODO: check quantities .

Low frequency density fluctuations may also be driven by a flute-like conducting-wall temperature-gradient instability which only requires an electron temperature gradient to grow (even with straight field lines)[41]. Simulations of turbulence in the LAPD suggest the possible presence of these conducting wall modes (CWM) which have the highest growth rate for $m \leq 20$[8]. This lower-m mode could be responsible for the peak around 3 kHz in the $M = 1$ I_{sat} fluctuation (fig. 10) and azimuthal mode numbers (fig. 15) and for the low-frequency low-$k_\parallel$ or flute-like behavior (fig. 11) . This CWM may also be responsible for an electron temperature profile (fig. 4) that is flatter than one would expect from the density profile. phil: Chapter 5 (page 75) of Friedman's thesis has statistical characteristics of this mode that fit this data. TODO: Calculate statistics from my data to directly compare with the simulations. Simulations predicted frequency and wavenumber spectra that can be fit with many power laws or exponentials[42] which are seen is these data (figs. 10, 12, 13).

These linearly unstable modes may be outgrown by a rapidly-growing nonlinear instability coupled to drift-like modes as suggested by simulations[8].

Troy: Good to dig out these other possible instabilities – can you comment on what these modes look like in all of the "fields" you measure – e.g. do they have appreciable magnetic fluctuations, etc?

C. Potential causes of particle flux reduction

The reduction in particle flux explained by a reduction in density fluctuations likely caused by a increased gradient scale length $L_n = \frac{n}{\nabla n}$ (fig. 9), decreasing the linear drift wave growth rate and thus saturation level. This gradient length reduction may also reduce the growth rate of the rotional interchange instability.

The decorrelation time of I_{sat} time series data is around 0.15 ms at x_{PF}. An estimate of the $E \times B$ flow shear from fig. 5 (DR2) yields a shearing time between 0.1 and 0.3 ms at x_{PF}. These times suggest that spontaneous flow shear may be important for suppressing turbulence at all mirror ratios as seen in other studies[6,43]. However, no clear trend in shearing strength is seen with mirror ratio, suggesting that the maximum turbulent transport may be fundamentally limited by flow shear but flow shear itself is not responsible for the decrease in I_{sat} fluctuation power or cross-field particle flux with mirror ratio. This interpretation is largely speculative because conclusive results would require direct, simultaneous measurements of decorrelation and shearing times.

It is important to note that the electron thermal diffusion time along the field line is very long compared to the frequency of the drift wave ($\omega \gtrsim k_\parallel \bar{v}_e^2/\nu_{ei}$)[44] so the electron temperature along the field line may not be constant on the drift wave timescale. This factor is not taken into account in this analysis but may have substantial impact on interpretations of the measured phase shift.

phil: Might just delete this sentence and bring it back if a reviewer has questions: The electrons are likely Boltzman because $\frac{\tilde{n}}{n} \approx \frac{\tilde{V}_f}{T_e} \approx \frac{\tilde{\Phi}}{T_e}$. $\frac{\tilde{V}_f}{T_e} \approx \frac{\tilde{\Phi}}{T_e}$ because triple probe measurements suggest T_e fluctuations are fairly small, though this may

contradict the hypothesized appearance of the conducting wall mode.

To fully determine the root cause of decreased fluctuation amplitudes, simulations are required. Also experiments with a fixed mirror well radius should also be conducted to better control the density scale length and its effect on drift waves and other instabilities

VI. CONCLUSIONS AND FUTURE WORK

TODO: Finish Future experiments in hotter regimes with the LaB6 cathode will need to be performed to evaluate the robustness of these results, particularly with stabilization of interchange. Additionally, the source field should also match the mirror midplane field so that the plasma remains the same radius, so geometric effects can be separated from plasma ones.

Simultaneous measurements using flux probes and I_{sat} are needed to accurately concretely determine if azimuthal flow shear is modified by the mirror field.

VII. ACKNOWLEDGEMENTS

TODO: Thanks to Troy, Gio, Pat, Steve for setting up probes and assisting with the datarun. Thanks to Mel Abler for insightful conversations. NSF/DOE

VIII. BIBLIOGRAPHY

[1]D. Endrizzi, J. Anderson, M. Brown, J. Egedal, B. Geiger, R. Harvey, M. Ialovega, J. Kirch, E. Peterson, Y. Petrov, J. Pizzo, T. Qian, K. Sanwalka, O. Schmitz, J. Wallace, D. Yakovlev, M. Yu, and C. Forest, "Physics basis for the Wisconsin HTS Axisymmetric Mirror (WHAM)," Journal of Plasma Physics **89**, 975890501 (2023).

[2]C. Forest, J. Anderson, D. Endrizzi, J. Egedal, S. Frank, K. Furlong, M. Ialovega, J. Kirch, R. Harvey, B. Lindley, Y. Petrov, J. Pizzo, T. Qian, K. Sanwalka, O. Schmitz, J. Wallace, D. Yakovlev, and M. Yu, "Prospects for a high-field, compact break-even axisymmetric mirror (BEAM) and applications," Journal of Plasma Physics **90**, 975900101 (2024).

[3]W. Horton, "Drift waves and transport," Reviews of Modern Physics **71**, 735–778 (1999).

[4]G. R. Tynan, A. Fujisawa, and G. McKee, "A review of experimental drift turbulence studies," Plasma Physics and Controlled Fusion **51**, 113001 (2009).

[5]D. A. Schaffner, T. A. Carter, G. D. Rossi, D. S. Guice, J. E. Maggs, S. Vincena, and B. Friedman, "Modification of Turbulent Transport with Continuous Variation of Flow Shear in the Large Plasma Device," Physical Review Letters **109**, 135002 (2012).

[6]D. A. Schaffner, T. A. Carter, G. D. Rossi, D. S. Guice, J. E. Maggs, S. Vincena, and B. Friedman, "Turbulence and transport suppression scaling with flow shear on the Large Plasma Device," Physics of Plasmas **20**, 055907 (2013).

[7]D. Schaffner, *Study of Flow, Turbulence and Transport on the Large Plasma Device*, Ph.D. thesis (2013).

[8]B. Friedman, T. A. Carter, M. V. Umansky, D. Schaffner, and I. Joseph, "Nonlinear instability in simulations of Large Plasma Device turbulence)," Physics of Plasmas **20**, 055704 (2013), https://pubs.aip.org/aip/pop/article-pdf/doi/10.1063/1.4805084/13856059/055704_1_online.pdf.

[9]F. M. Poli, S. Brunner, A. Diallo, A. Fasoli, I. Furno, B. Labit, S. H. Müller, G. Plyushchev, and M. Podestà, "Experimental characterization of drift-interchange instabilities in a simple toroidal plasma," Physics of Plasmas **13**, 102104 (2006).

[10]A. Fasoli, B. Labit, M. McGrath, S. H. Müller, G. Plyushchev, M. Podestà, and F. M. Poli, "Electrostatic turbulence and transport in a simple magnetized plasma," Physics of Plasmas **13**, 055902 (2006).

[11]A. Mase, A. Itakura, M. Inutake, K. Ishii, J. Jeong, K. Hattori, and S. Miyoshi, "Control of the radial electric field and of turbulent fluctuations in a tandem mirror plasma," Nuclear Fusion **31**, 1725 (1991).

[12]M. Yoshikawa, Y. Miyata, M. Mizuguchi, N. Imai, H. Hojo, M. Ichimura, T. Kariya, I. Katanuma, Y. Nakashima, R. Minami, H. Shidara, Y. Yamaguchi, Y. Shima, Y. Ohno, F. Yaguchi, and T. Imai, "Use of a Gold Neutral Beam Probe to Study Fluctuation Suppression During Potential Formation in the GAMMA 10 Tandem Mirror," Fusion Science and Technology **57**, 312–319 (2010).

[13]F. Brochard, E. Gravier, and G. Bonhomme, "Transition from flute modes to drift waves in a magnetized plasma column," Physics of Plasmas **12**, 062104 (2005).

[14]J. Hooper, E. B., D. E. Baldwin, T. K. Fowler, R. J. Kane, and W. C. Turner, "Radial transport reduction in tandem mirrors using end-wall boundary conditions," The Physics of Fluids **27**, 2264–2267 (1984), https://pubs.aip.org/aip/pfl/article-pdf/27/9/2264/12418415/2264_1_online.pdf.

[15]P. Bagryansky, A. Lizunov, A. Zuev, E. Y. Kolesnikov, and A. Solomachin, "Experiments with Controllable Application of Radial Electric Fields in GDT Central Cell," Fusion Science and Technology **43**, 152–156 (2003).

[16]P. Bagryansky, A. Beklemishev, and E. Soldatkina, "Influence of Radial Electric Field on High-Beta Plasma Confinement in the Gas Dynamic Trap," Fusion Science and Technology **51**, 340–342 (2007).

[17]A. D. Beklemishev, P. A. Bagryansky, M. S. Chaschin, and E. I. Soldatkina, "Vortex Confinement of Plasmas in Symmetric Mirror Traps," Fusion Science and Technology **57**, 351–360 (2010).

[18]W. Gekelman, P. Pribyl, Z. Lucky, M. Drandell, D. Leneman, J. Maggs, S. Vincena, B. Van Compernolle, S. K. P. Tripathi, G. Morales, T. A. Carter, Y. Wang, and T. DeHaas, "The upgraded Large Plasma Device, a machine for studying frontier basic plasma physics," Review of Scientific Instruments **87**, 025105 (2016).

[19]Y. Qian, W. Gekelman, P. Pribyl, T. Sketchley, S. Tripathi, Z. Lucky, M. Drandell, S. Vincena, T. Look, P. Travis, T. Carter, G. Wan, M. Cattelan, G. Sabiston, A. Ottaviano, and R. Wirz, "Design of the Lanthanum hexaboride based plasma source for the large plasma device at UCLA," Review of Scientific Instruments **94**, 085104 (2023), https://pubs.aip.org/aip/rsi/article-pdf/doi/10.1063/5.0152216/18074441/085104_1_5.0152216.pdf.

[20]E. Powers, "Spectral techniques for experimental investigation of plasma diffusion due to polychromatic fluctuations," Nuclear Fusion **14**, 749 (1974).

[21]T. A. Carter and J. E. Maggs, "Modifications of turbulence and turbulent transport associated with a bias-induced confinement transition in the Large Plasma Device," Physics of Plasmas **16**, 012304 (2009).

[22]J. E. Maggs, T. A. Carter, and R. J. Taylor, "Transition from Bohm to classical diffusion due to edge rotation of a cylindrical plasma," Physics of Plasmas **14**, 052507 (2007), https://pubs.aip.org/aip/pop/article-pdf/doi/10.1063/1.2722302/13884683/052507_1_online.pdf.

[23]J. E. Maggs and G. J. Morales, "Fluctuations associated with a filamentary density depletion," Physics of Plasmas **4**, 290–299 (1997).

[24]S. Vincena and W. Gekelman, "Drift-Alfvén wave mediated particle transport in an elongated density depression," Physics of Plasmas **13**, 064503 (2006).

[25]A. Mallet, S. Dorfman, M. Abler, T. A. Bowen, and C. H. K. Chen, "Nonlinear dynamics of small-scale Alfvén waves," Physics of Plasmas **30**, 112102 (2023), https://pubs.aip.org/aip/pop/article-pdf/doi/10.1063/5.0151035/18196013/112102_1_5.0151035.pdf.

[26]J. V. Hollweg, "Kinetic alfvén wave revisited," Journal of Geophysical Research: Space Physics **104**, 14811–14819 (1999), https://agupubs.onlinelibrary.wiley.com/doi/pdf/10.1029/1998JA900132.

[27]J. E. Maggs, G. J. Morales, and T. A. Carter, "An Alfvén wave maser in the laboratory," Physics of Plasmas **12**, 013103 (2005).

[28]M. Wakatani and A. Hasegawa, "A collisional drift wave de-

scription of plasma edge turbulence," The Physics of Fluids **27**, 611–618 (1984), https://pubs.aip.org/aip/pfl/article-pdf/27/3/611/12476138/611_1_online.pdf.

[29]J. M. Beall, Y. C. Kim, and E. J. Powers, "Estimation of wavenumber and frequency spectra using fixed probe pairs," Journal of Applied Physics **53**, 3933–3940 (1982), https://pubs.aip.org/aip/jap/article-pdf/53/6/3933/18397748/3933_1_online.pdf.

[30]A. A. Ivanov and V. V. Prikhodko, "Gas-dynamic trap: an overview of the concept and experimental results," Plasma Physics and Controlled Fusion **55**, 063001 (2013).

[31]T. A. Casper and G. R. Smith, "Observation of alfvén ion-cyclotron fluctuations in the end-cell plasma in the tandem mirror experiment," Phys. Rev. Lett. **48**, 1015–1018 (1982).

[32]T. C. Simonen, "Measurements of ion cyclotron instability characteristics in a mirror-confined plasma," The Physics of Fluids **19**, 1365–1370 (1976), https://pubs.aip.org/aip/pfl/article-pdf/19/9/1365/12452724/1365_1_online.pdf.

[33]B. Kanaev, "Stabilization of drift loss-cone instability (dci) by addition of cold ions," Nuclear Fusion **19**, 347 (1979).

[34]R. Post, "The magnetic mirror approach to fusion," Nuclear Fusion **27**, 1579 (1987).

[35]D. D. Ryutov, H. L. Berk, B. I. Cohen, A. W. Molvik, and T. C. Simonen, "Magneto-hydrodynamically stable axisymmetric mirrors," Physics of Plasmas **18**, 092301 (2011), https://pubs.aip.org/aip/pop/article-pdf/doi/10.1063/1.3624763/16708540/092301_1_online.pdf.

[36]B. Van Compernolle, W. Gekelman, P. Pribyl, and C. M. Cooper, "Wave and transport studies utilizing dense plasma filaments generated with a lanthanum hexaboride cathode," Physics of Plasmas **18**, 123501 (2011), https://pubs.aip.org/aip/pop/article-pdf/doi/10.1063/1.3671909/16114892/123501_1_online.pdf.

[37]S. Fornaca, Y. Kiwamoto, and N. Rynn, "Experimental stabilization of interchange mode by surface line tying," Phys. Rev. Lett. **42**, 772–776 (1979).

[38]G. E. Guest and E. G. Harris, "Flute stabilization via electrostatically confined cold electrons," Phys. Rev. Lett. **27**, 1500–1503 (1971).

[39]A. Komori, Y. Higuchi, Y. Suetsugu, A. Yonesu, and Y. Kawai, "Flute stabilization of a mirror-confined plasma by a positive ambipolar potential," Journal of the Physical Society of Japan **56**, 2607–2610 (1987), https://doi.org/10.1143/JPSJ.56.2607.

[40]P. Popovich, M. V. Umansky, T. A. Carter, and B. Friedman, "Analysis of plasma instabilities and verification of the BOUT code for the Large Plasma Device," Physics of Plasmas **17**, 102107 (2010).

[41]H. L. Berk, D. D. Ryutov, and Y. A. Tsidulko, "Temperature-gradient instability induced by conducting end walls," Physics of Fluids B: Plasma Physics **3**, 1346–1354 (1991).

[42]B. C. Friedman, *Simulation Analysis of Zero Mean Flow Edge Turbulence in LAPD*, Ph.D. thesis (2013).

[43]T. Cho, M. Yoshida, J. Kohagura, M. Hirata, T. Numakura, H. Higaki, H. Hojo, M. Ichimura, K. Ishii, K. M. Islam, A. Itakura, I. Katanuma, Y. Nakashima, T. Saito, Y. Tatematsu, M. Yoshikawa, Y. Kojima, S. Tokioka, N. Yokoyama, Y. Tomii, T. Imai, V. P. Pastukhov, and S. Miyoshi, "Observation of the Effects of Radially Sheared Electric Fields on the Suppression of Turbulent Vortex Structures and the Associated Transverse Loss in GAMMA 10," Physical Review Letters **94**, 085002 (2005).

[44]R. Goldston, *Introduction to Plasma Physics* (CRC Press, Boca Raton, 1995).

[45]C. Perks, S. Mordijck, T. Carter, B. Van Compernolle, S. Vincena, G. Rossi, and D. Schaffner, "Impact of the electron density and temperature gradient on drift-wave turbulence in the Large Plasma Device," Journal of Plasma Physics **88**, 905880405 (2022).